Self-Assembly of Nitrogen-Rich Conjugated Metal–Organic and Organic Macrocycles

Phuong H. Le,[†] Leo B. Zasada,[†] Jackson Geary,[†] Ashlyn A. Kamin,[†] Audrey M. Hill,[†] Dianne J. Xiao[†,*]

[†] Department of Chemistry, University of Washington, Seattle, Washington 98195-1700, United States
* Correspondence to: djxiao@uw.edu

Abstract: Here we report the synthesis of nitrogen-rich conjugated metal–organic and organic macrocycles that resemble truncated fragments of semiconducting 2D metal–organic and covalent organic frameworks. Key to the self-assembly of these new shape-persistent macrocycles is the development of a versatile bis(alkoxy)-tetraaminotriphenylene building block, H_4TNTP-OC4, which is compatible with diverse coordination chemistry and dynamic covalent chemistry reactions. Combining H_4TNTP-OC4 with nickel(II) salts leads to nickel-based metal–organic macrocycles, while reaction with tetraketones leads to pyrazine-based organic macrocycles. The fully conjugated macrocycle core supports strong interlayer stacking, out-of-plane charge transport, and well-defined nanochannels, while the macrocycle periphery provides new opportunities for atomically precise surface engineering. In particular, the nickel macrocycles display pressed pellet conductivities on the order of 10^{-3} S/cm and a surface area of 130 m^2/g. Together, these structures show how simple macrocycles can preserve key properties of 2D crystalline frameworks while offering greater surface tunability.

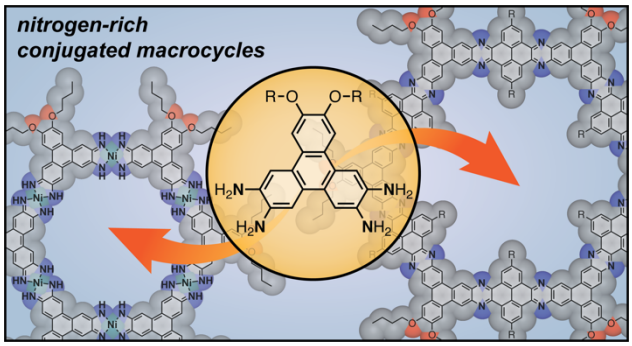

Introduction:

There has been rising recent interest in downsizing porous crystalline frameworks to the nanoscale.[1–3] At the extreme limit of this endeavor is the construction of discrete molecular cages and macrocycles whose structures mimic individual pores found in bulk metal–organic and covalent organic frameworks.[4–8] These nanosized molecules often retain the original function and porosity found in their parent frameworks while introducing new properties. For example, the greater solution processability of cages and macrocycles aids their integration into thin film electronic devices[9,10] and membranes.[11–13] Soluble porous molecules also enable the formation of new composite materials, such as the use of charged metal–organic cages to achieve solid porous salts with tunable compositions.[14] Finally, porous molecules can undergo much greater structural changes in response to stimuli, such as the reversible self-assembly and dissolution of aggregated architectures.[15–17]

Our lab has been interested in truncating two-dimensional semiconducting metal–organic frameworks (MOFs) and covalent organic frameworks (COFs) into discrete macrocycles that merge the physical properties of crystalline frameworks with the processability of soft materials.[9] For example, we recently used the ditopic ligand H_4TOTP-OR (H_4TOTP = 2,3,6,7-tetrahydroxytriphenylene, OR = linear C2, C4, C6, and C18 alkoxy chains) to construct conjugated copper macrocycles that resemble the 2D metal–organic framework $Cu_3(HHTP)_2$ (HHTP =

2,3,6,7,10,11-hexahydroxytriphenylene).[9] The macrocycles self-assemble into π-stacked nanotubes that preserve the porosity and out-of-plane charge transport found in $Cu_3(HHTP)_2$.

In this work, we expand upon our previous studies by introducing a new ditopic triphenylene-based ligand containing nitrogen bridging atoms (**Fig. 1**). Nitrogen donor groups are intriguing from both an organic and an inorganic materials perspective. In the context of semiconducting metal–organic materials, nitrogen donors provide superior charge transport properties relative to oxygenated analogues due to increased metal–ligand covalency. In the context of organic materials, the greater nucleophilicity of nitrogen compared to oxygen provides access to a wider range of bond-forming reactions. For example, *o*-phenylenediamine units can react with 1,2-diketones, aldehydes, and *ortho*-difluorinated aromatic compounds to form pyrazine,[18–22] imidazole,[23,24] and piperazine[25,26] linkages, respectively (**Fig. 1a**). These reactions have been exploited in both metal–organic framework and covalent organic framework chemistry to achieve semiconducting materials with high chemical and thermal stability.

Here we show that the ditopic ligand H_4TNTP-OC4 (H_4TNTP-OC4 = 10,11-dibutoxytriphenylene-2,3,6,7-tetraamine) can be used to construct nitrogen-rich conjugated metal–organic and organic macrocycles that resemble semiconducting 2D MOFs and COFs in both form and function (**Fig. 1b**). Combining H_4TNTP-OC4 and nickel(II) salts produces conductive nickel macrocycles with Brunauer–Emmett–Teller (BET) surface areas of 130 m^2/g and pellet conductivities of 5(1) $\times 10^{-3}$ S/cm. Similarly, reacting H_4TNTP-OC4 with either pyrene-4,5,9,10-tetraone or its di-*tert*-butyl substituted variant forms pyrazine-linked conjugated organic macrocycles, which are structurally confirmed by powder X-ray diffraction, vibrational spectroscopy, and solid-state ^{13}C NMR. The development of nitrogen-rich ligands such as

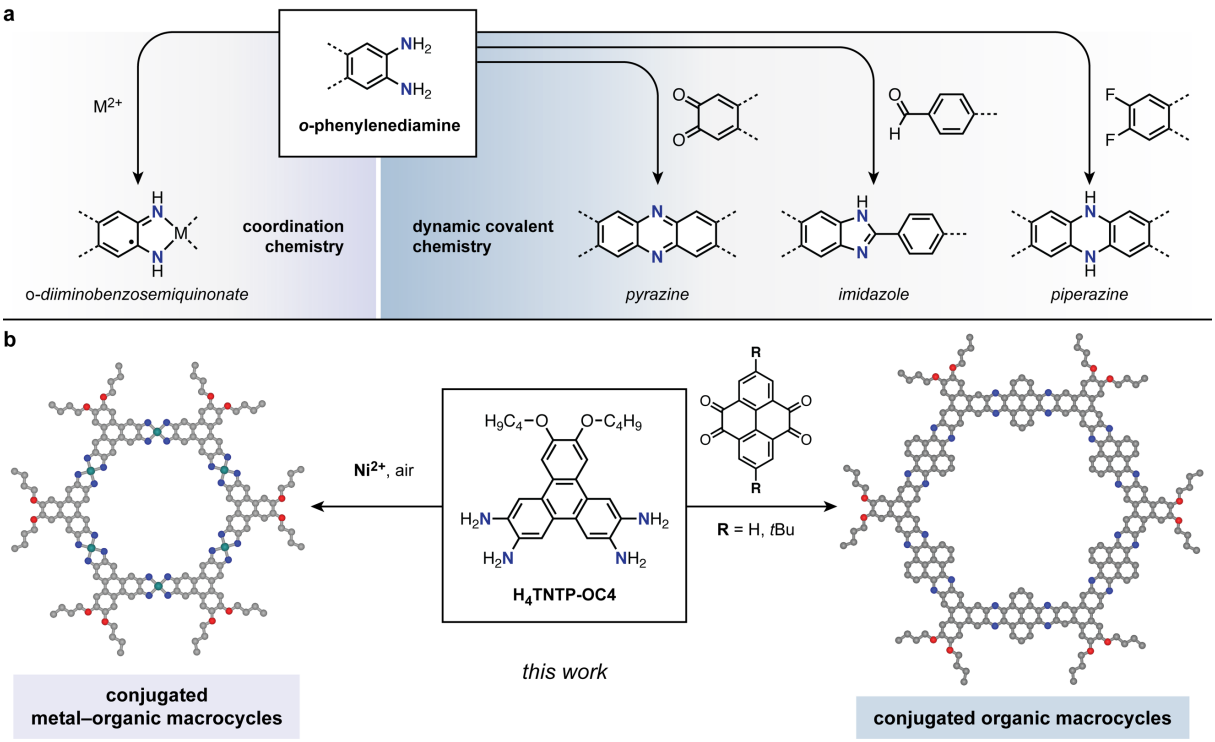

Fig. 1 | (a) Schematic illustration of the different linkages that can be formed from *o*-phenylenediamine precursors via coordination chemistry and dynamic covalent chemistry. (b) Construction of metal–organic macrocycles and conjugated organic macrocycles starting from the bis(alkoxy)-tetraaminotriphenylene ligand, H_4TNTP-OC4.

H_4TNTP-OC4 greatly expands the diversity of conjugated macrocyclic structures that can be obtained by coordination and dynamic covalent chemistry.

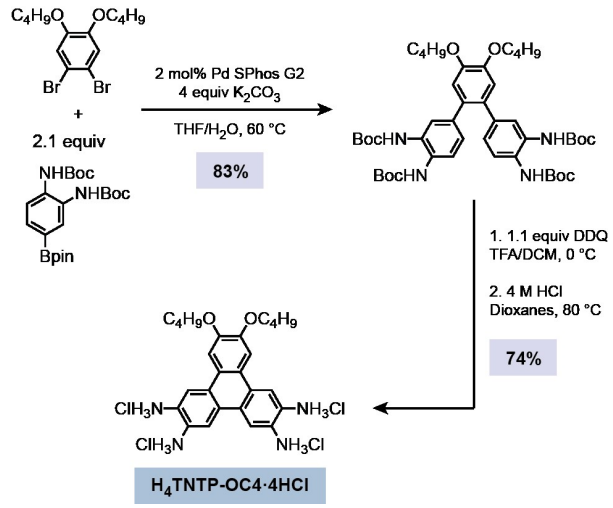

Fig. 2 | Synthesis of the H_4TNTP-OC4 ligand via Suzuki coupling followed by DDQ catalyzed ring closure and BOC protecting group removal.

Ligand design. We envisioned that bis(alkoxy)-tetraaminotriphenylene ligands could be synthesized following a similar route as the one developed by Northrop and coworkers for bis(alkoxy)-tetrahydroxytriphenylenes.[27] Their approach relies on Suzuki coupling to synthesize *ortho*-terphenyl precursors containing *tert*-butyldimethylsilyl (TBDMS)-protected catechols, which are subsequently oxidatively cyclized and deprotected. We hypothesized that simply replacing the TBDMS-protected catechols with tert-butoxycarbonyl (BOC)-protected *o*-phenylenediamine coupling partners would generate the desired nitrogen-based ligands. Gratifyingly, the proposed synthetic route proceeded smoothly. The desired bis(butoxy)-tetraaminotriphenylene ligand was isolated as the protonated hydrochloride salt (H_4TNTP-OC4·4HCl) in 61% overall yield over three steps (**Fig. 2**). Note that the H_4TNTP-OC4 ligand is always isolated and handled in its protonated form (H_4TNTP-OC4·4HCl) to minimize oxidative degradation. While this work focuses on ligands containing *n*-butyl side chains, the modular synthetic route should allow the peripheral side chains to be readily tuned in future studies.

Synthesis and characterization of nickel macrocycles. Dincă and coworkers reported the first nitrogen-based conjugated 2D metal–organic framework $Ni_3(HITP)_2$ (HITP = 2,3,6,7,10,11-hexaiminotriphenylene) in 2014,[28] with a subsequent follow-up study on mixed-metal variants in 2020.[29] Recent single crystal measurements have shown that the out-of-plane conductivity in $Ni_3(HITP)_2$ is ~100-fold higher than similar 2D frameworks containing oxygen-based ligands, such as $Cu_3(HHTP)_2$.[30–32] Due to these favorable properties, $Ni_3(HITP)_2$ has been explored for diverse applications, including electrochemical energy storage,[33] electrocatalysis,[34,35] and chemical sensing.[36,37] Given the rich chemistry observed in this particular member of the conjugated 2D MOF family, we were excited to explore the properties of its macrocyclic form.

The addition of an external base is critical to the synthesis of $M_3(HITP)_2$ materials.[28,29] In particular, it is common to add a large excess of an alkali acetate salt (>100 equiv) to the synthesis mixture, where it serves both as a weak base to deprotonate the ligand, as well as a coordination modulator to improve crystallinity.[29] Combining 1 equiv H_4TNTP-OC4·4HCl, 1.5 equiv $Ni(OAc)_2$, and 10 equiv of an aqueous MOAc solution ($M^+ = Na^+, K^+$) in DMSO led to moderately crystalline material (**Fig. S2**). However, further increasing the equivalents of MOAc to 100 reduced the crystallinity, leading to amorphous material (**Fig. S3**). We hypothesized this was due to the unusual solubility characteristics of our ligand, which contains highly polar ammonium groups as well as hydrophobic alkyl chains. Because of the alkyl chains, even small amounts of water in the reaction mixture led to rapid precipitation.

We found that two important reaction conditions were necessary to obtain highly crystalline material. First, we switched to tetrabutylammonium acetate (TBAOAc) as our acetate source. The tetrabutylammonium cation has much greater solubility in organic solvents, allowing us to avoid the use of aqueous solutions. Second, we found that DMSO was a uniquely enabling solvent for this reaction. No precipitate was formed when DMA was used, and an amorphous solid was obtained in DMF. We note that omitting the acetate was also not acceptable; no precipitate formed in the absence of external base even after a reaction time of one month.

Heating 1 equiv H_4TNTP-OC4·4HCl, 1.5 equiv $Ni(OAc)_2$, and 10 equiv of TBAOAc in DMSO at 65 °C for 24 h produced a highly crystalline dark blue-black powder (**Fig. 3**). The first three peaks at 2θ = 2.70, 4.68, and 5.40° follow the 1:1/√3:1/2 ratio in d-spacing expected for a hexagonal unit cell (**Fig. 3c**). Based on the position of the first peak, an approximate *a* and *b* dimension of 37.8 Å was obtained. This value is nearly identical to the dimensions of a fully relaxed, geometry optimized model of NiTNTP-OC4 obtained using the Forcite module in Materials Studio ($a = b$ = 37.92 Å). Finally, a broad peak centered at 27.1° is observed, which we have assigned as the π–π stacking feature. This peak corresponds to a short distance of ~3.3 Å, which is consistent with both the strong π–π stacking found in the parent framework $Ni_3(HITP)_2$ (~3.3 Å)[30] as well as our previously reported copper-based metal–organic macrocycles (~3.2 Å).[9] While structurally similar 2D MOFs are known to favor either eclipsed or slightly slipped arrangements,[29,30] we note that our material is not sufficiently crystalline to rule out other packing motifs.

High-resolution X-ray photoelectron spectroscopy (XPS) measurements were carried out to further probe the chemical environment of our macrocycles and support our structural assignment. Analysis of the Ni 2p spectrum shows a binding energy of ~855 eV for the Ni $2p_{3/2}$ peak and ~873 eV for the $2p_{1/2}$ peak, consistent with a Ni(II) oxidation state (**Fig. 3d**).[38] Importantly, very faint satellite features are observed, as expected for diamagnetic, square planar Ni(II) sites.[38] We note that the presence of weak satellite features is likely due to solvent binding at surface sites or other defects, as similar features are also observed in nanocrystalline $Ni_3(HITP)_2$.[29,39]

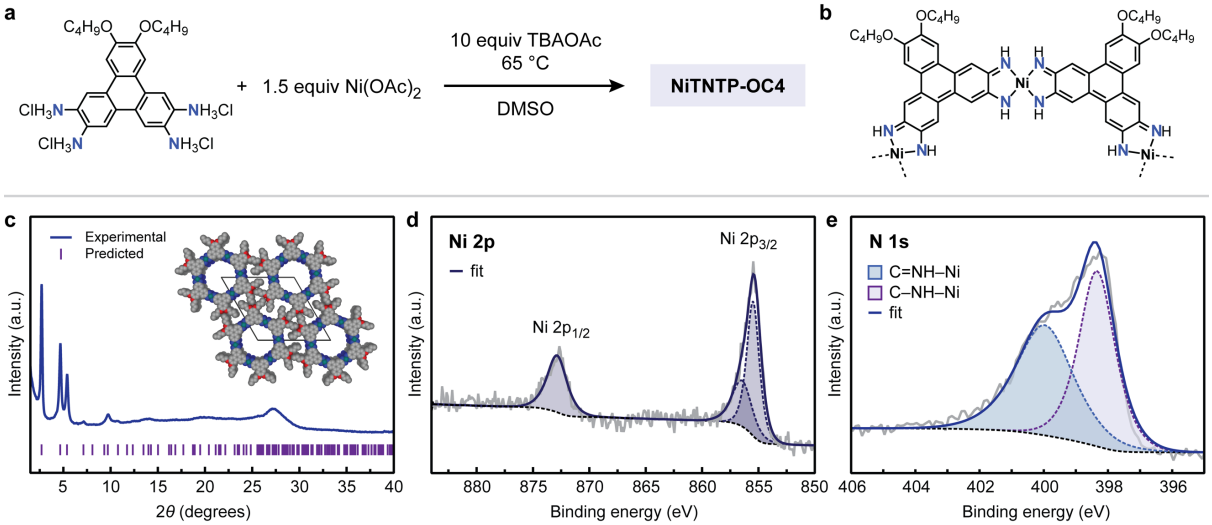

Fig. 3 | (a) Synthesis of NiTNTP-OC4. (b) Proposed structure of NiTNTP-OC4, highlighting the partially oxidized ligand. (c) Experimental powder X-ray diffraction pattern of NiTNTP-OC4 along with modeled structure and predicted diffraction peaks. (d) High resolution Ni 2p XPS spectrum, showing the absence of satellite features. (e) High resolution N 1s XPS spectrum, showing the presence of two distinct nitrogen environments.

In the extended framework $Ni_3(HITP)_2$, it is proposed that each of the three *o*-phenylenediamine units is doubly deprotonated and oxidized by 1 e^- to generate monoanionic, *o*-diiminobenzosemiquinonate sites (**Fig. 1a**). Because our ligand only has two *o*-phenylenediamine units, we propose that a diamagnetic, partially oxidized ligand containing distinct imine and amine units is formed rather than a diradical species (**Fig. 3b**). This assignment is supported by our N 1s XPS data (**Fig. 3e**). The spectrum can be fit well with two distinct peaks of equal area, one at ~400 eV and a second at ~398 eV. We assign the peak at ~400 eV to the oxidized imine group (C=NH–M), and the lower energy peak to unoxidized amine (C–NH–M).[40]

Interestingly, the structure of NiTNTP-OC4 is considerably less sensitive to solvation state than related triphenylene-based macrocycles, such as our previously reported CuTOTP-OR macrocycles[9] and Dichtel and coworkers' boronate ester-linked macrocycles.[41] Minimal changes to the unit cell dimensions (<5%) and peak broadness (5% decrease in FWHM) are observed upon soaking NiTNTP-OC4 in DMA and drying the material under vacuum (**Fig. S5** and **Table S2**). In contrast, the diffraction pattern of CuTOTP-OC4 broadens significantly upon drying (28% increase in FWHM), while the *a* and *b* unit cell dimensions of boronate ester-linked macrocycles contract by nearly 10 Å upon desolvation (~18% decrease).[41]

The less dynamic structure of NiTNTP-OC4 suggests the material may have more robust interlayer and intercolumn interactions, which should promote porosity and electrical conductivity. Indeed, gas sorption measurements show that the interior channels remain accessible to guest molecules after desolvation. A BET surface area of 130 m^2/g was obtained from 273 K CO_2 adsorption isotherms. Excitingly, pressed pellet conductivity measurements provided an average conductivity of $5(1) \times 10^{-3}$ S/cm, which is an order of magnitude higher than our previously reported CuTOTP-OC4 macrocycle ($6(2) \times 10^{-4}$ S/cm). This increase is consistent with previously reported single crystal conductivity measurements on the analogous metal–organic frameworks, which show that the conductivity of $Ni_3(HITP)_2$ rods (~150 S/cm) is approximately two orders of magnitude higher than $Cu_3(HHTP)_2$ rods (~1.5 S/cm).[30]

Together, these results show that metal–organic macrocycles, like the MOFs that inspired their synthesis, are highly tunable. The use of alternative metals and bridging atoms can be leveraged to achieve new families of materials with similar structures but greatly improved charged transport properties. Finally, we note that the macrocycle periphery can also be tailored towards a specific function. For example, while NiTNTP-OC4 shows relatively poor colloidal stability in its current form (**Table S5** and **Fig. S10**), side-chain engineering should greatly improve the processability of these materials. Analogous *n*-butyl-functionalized copper macrocycles were shown to be similarly prone to aggregation but could be rendered fully soluble in organic solvents with the addition of longer C18 alkyl chains.[9]

Synthesis and characterization of pyrazine-based macrocycles. After successfully synthesizing metal–organic macrocycles using H_4TNTP-OC4, we hypothesized that the same ligand could also be used to form truncated analogues of covalent organic frameworks. As a proof-of-concept, we targeted the synthesis of pyrazine-linked macrocycles, as their COF counterparts have become an important and widely studied class of semiconducting crystalline frameworks. The first pyrazine-linked covalent organic framework was synthesized by Jiang and coworkers in 2013 by combining 2,3,6,7,10,11-hexaaminotriphenylene and 2,7-di-*tert*-butylpyrene-4,5,9,10-tetraone.[18] This synthesis led to a fully conjugated structure that was not only much more chemically robust than traditional boronate ester and imine-based COFs, but also afforded p-type semiconducting behavior. Since this initial report, additional pyrazine-linked conjugated covalent

organic frameworks have been reported[19–22] and studied as active materials in transistors,[19] chemiresistive sensors,[20] and battery cathode materials.[22]

While some syntheses of pyrazine-linked COFs employ basic conditions,[22] the vast majority use acidic modulators such as acetic acid and sulfuric acid. Heating H_4TNTP-OC4·4HCl (1.2 equiv) and pyrene-4,5,9,10-tetraone (1 equiv) in 1:1 acetic acid/DMF at 120 °C under an N_2 atmosphere produced PyrTNTP-OC4 (pyr = pyrazine) as a brown crystalline solid (**Fig. 4a** and **Fig. S11**). Overall, the observed experimental powder X-ray diffraction pattern is broadly consistent with structural models optimized in a hexagonal packing arrangement (**Fig. S11**). The first peak is located at 2θ = 2.36°, indicating a large *a* and *b* unit cell dimension of 43.2 Å, as expected for a large organic macrocycle with >2 nm pore windows. Furthermore, an intense peak is observed at 26.7°, which we have assigned as the π–π stacking feature. This peak corresponds to a distance of 3.3 Å, which is comparable to the ~3.3–3.5 Å range of π–π stacking distances observed in other planar pyrazine-linked COFs.[19–22]

Excitingly, the synthesis could be extended to di-*tert*-butyl functionalized pyrene-4,5,9,10-tetraone coupling partners as well. Combining H_4TNTP-OC4·4HCl (1.5 equiv) and 2,7-di-*tert*-butylpyrene-4,5,9,10-tetraone (1 equiv) in 1:10 H_2SO_4/NMP at 150 °C under an N_2 atmosphere produced tBu-PyrTNTP-OC4 as a dark reddish brown crystalline solid (**Fig. 4**). The first four diffraction peaks are located at 2θ = 2.74, 4.72, 5.44, and 7.22°, consistent with the expected 1:1/√3:1/2:1/√7 ratio in *d*-spacing for a hexagonal unit cell (**Fig. 4b**). A weak, broad peak around $2\theta \sim$ 25–26° is observed, corresponding to a π–π stacking distance of ~3.5 Å. This is slightly larger than the ~3.3 Å observed in PyrTNTP-OC4, which is expected given the bulkier *tert*-butyl substituents. After drying under vacuum at room temperature, the π–π stacking feature at ~25–26° becomes more well-defined while the other peaks broaden (**Fig. S12**). Interestingly, the position of the first peak shifts from 2.74° to 2.44° upon drying, corresponding to an expansion of the *a*

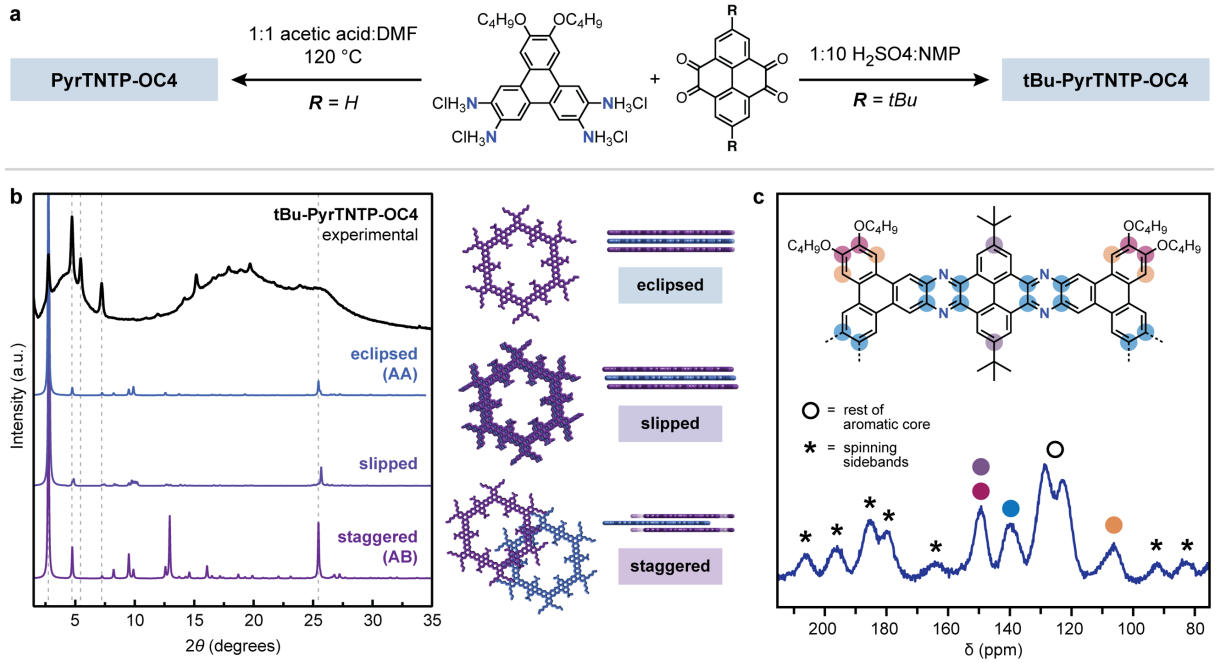

Fig. 4 | (a) Synthesis of two pyrazine-based conjugated macrocycles, PyrTNTP-OC4 and tBu-PyrTNTP-OC4. (b) Experimental powder X-ray diffraction pattern alongside predicted diffraction patterns for tBu-PyrTNTP-OC4 with eclipsed, slipped, and staggered π–π stacking motifs. (c) Solid-state ^{13}C NMR spectrum of tBu-PyrTNTP-OC4. Asterisks denote the spinning sidebands.

and *b* unit cell dimensions from 37.2 Å to 41.8 Å. We hypothesize that this expansion is due to changes in the packing of the *n*-butyl side chains, particularly as the material desolvates and the π–π stacking becomes more ordered.

Given the relatively broad diffraction peaks, the exact π–π stacking arrangements adopted by PyrTNTP-OC4 and tBu-PyrTNTP-OC4 are difficult to determine with absolute certainty. Previously reported computational studies on 2D covalent organic frameworks have shown that slipped (also called inclined) and serrated structures with small interlayer offsets are more energetically favored than perfectly eclipsed arrangements.[42] On the other hand, the experimental peak intensities of solvated 2D COFs are better modeled with larger interlayer offsets ("quasi-AB").[43] Similarly, frameworks with larger alkyl substituents have been shown to adopt fully staggered AB and ABC stacking motifs.[44] Considering the relative peak intensities as well as the presence of sterically bulky *tert*-butyl groups, we hypothesize that tBu-PyrTNTP-OC4 likely adopts either a quasi-AB or AB stacking pattern (**Fig. 4b**).

The successful formation of pyrazine linkages was confirmed spectroscopically through a combination of infrared spectroscopy and solid-state ^{13}C NMR (**Fig. 4c**). The infrared spectrum of PyrTNTP-OC4 shows the disappearance of the amine N–H stretches and the preservation of the alkyl C–H features, confirming that the H_4TNTP-OC4 backbone is present but the free amine groups have reacted (**Fig. S13**). Surprisingly, a carbonyl C=O stretching feature at 1660 cm^{-1} is observed in PyrTNTP-OC4, which cannot be removed even after repeating rinsing with solvents such as DMF, MeOH, and DCM. We attribute this feature to a small number of unreacted, dangling carbonyl groups and incomplete macrocyclization. Similar residual C=O stretches have been observed in related pyrazine-based COFs[22] and are likely exacerbated by the poor solubility of pyrene-4,5,9,10-tetraone. Consistent with this hypothesis, the residual C=O stretches are significantly reduced in tBu-PyrTNTP-OC4 due to the greater solubility afforded by the *tert*-butyl substituents (**Fig. S14**).

While the dibenzopyrazine ring system is known to display characteristic stretches between 1200–1500 cm^{-1},[18,20,21] these bands were difficult to definitively assign due to the large number of peaks in this region. Vibrational frequency calculations using density functional theory show that this region of the spectra is populated by a large number of skeletal vibrations involving the entirety of the macrocycle core (see **Fig. S15** and the SI for more details). Therefore, we turned to solid-state ^{13}C NMR to confirm the presence of pyrazine linkages, as pyrazine moieties have a diagnostic peak at ~140 ppm.[18,21,22] Gratifyingly, a new peak at 139.8 ppm is observed in the solid-state ^{13}C NMR spectrum of both PyrTNTP-OC4 and tBu-PyrTNTP-OC4 that is not present in the starting ligand (**Fig. 4c and Fig. S17–18)**, confirming the formation of a dibenzopyrazine unit. Consistent with our infrared spectra, a residual carbonyl peak is observed at 172.8 ppm in PyrTNTP-OC4 but is completely absent in the ^{13}C NMR of tBu-PyrTNTP-OC4 (**Fig. 4c** and **Fig. S17**).

Preliminary pressed pellet conductivity measurements show that tBu-PyrTNTP-OC4 is semiconducting, with a modest electrical conductivity of $8(1) \times 10^{-10}$ S/cm. This is consistent with previously reported conjugated 2D COFs, which generally display relatively low pellet conductivities of 10^{-10} to 10^{-5} S/cm prior to chemical doping.[45,46] Orders of magnitude increases in conductivity can be observed upon p-type doping with chemical oxidants,[46] which will be the subject of future work.

Finally, we tested the dispersibility of tBu-PyrTNTP-OC4 in organic solvents. Immediately after synthesis, the material was isolated by centrifugation, washed with DMF, and redispersed in a variety of organic solvents (DMF, DCM, MeOH, THF, and toluene) via probe sonication. We note that isolating the material via centrifugation, and not filtration, was important to maintaining

dispersibility. Out of the five solvents tested, tBu-PyrTNTP-OC4 formed the most stable colloidal dispersions in DCM (**Fig. S19** and **Fig. S20**). Dynamic light scattering (DLS) measurements immediately following sonication showed that over 90% of the particles were less than 100 nm in diameter, with a smaller population of ~500 nm particles (**Table S6**). This particle size distribution remained relatively constant over the course of 24 hours. However, we note that the population of larger ~400–500 nm particles does increase over the period of two weeks, indicating slow aggregation over time.

The relative ease by which tBu-PyrTNTP-OC4 can be dispersed in organic solvents highlights the processability advantages of discrete macrocycles over structurally similar extended 2D frameworks. While colloidally stable imine- and boronate ester-based COF nanoparticles have been reported,[47–49] to our knowledge similar syntheses have not been developed for pyrazine-based COFs. This may be due to their exceptionally strong π–π stacking and relatively harsh synthesis conditions. Going forward, the greater dispersibility of tBu-PyrTNTP-OC4 may aid the integration of these materials in thin film membranes and electrochemical devices, as well as facilitate more intimate mixing with binders and conductive additives.

Conclusion.

In conclusion, we have developed a new nitrogen-based ditopic ligand, H_4TNTP-OC4, which is compatible with diverse coordination chemistry and dynamic covalent chemistry reactions. Using this versatile building block, we have constructed three fully conjugated and shape-persistent macrocyclic cores with strong interlayer stacking, semiconducting behavior, and high chemical stability. Specifically, metalating H_4TNTP-OC4·4HCl with nickel(II) salts leads to fully conjugated nickel macrocycles with pressed pellet conductivities on the order of 10^{-3} S/cm.[9] These values are ten-fold higher than related macrocycles constructed from oxygen-based ligands. Similarly, the reaction of H_4TNTP-OC4·4HCl with tetraketones leads to a new family of fully conjugated organic macrocycles containing robust pyrazine linkages, strong interlayer π–π stacking, and good solution processability. Together, the work outlined here further emphasizes how discrete conjugated macrocycles can preserve key structural features of 2D metal–organic and covalent organic frameworks while enabling new directions in synthetic and materials chemistry.

Acknowledgements.

Materials synthesis efforts were supported by the U.S. Department of Energy, Office of Science, Office of Basic Energy Sciences under Award Number DE-SC0021966. Additional characterization efforts were supported by the Arnold and Mabel Beckman Foundation through a Beckman Young Investigator Award and the David and Lucile Packard Foundation. P.H.L. was supported in part by the state of Washington through graduate fellowships from the University of Washington Clean Energy Institute. J.G. and A.A.K. were supported by NSF graduate research fellowship. The authors acknowledge the use of instrumentation at the following shared facilities: the Washington Research Training Testbeds, a facility operated by the University of Washington Clean Energy Institute; the Molecular Analysis Facility, a National Nanotechnology Coordinated Infrastructure (NNCI) site at the University of Washington, which is supported in part by funds from the National Science Foundation (awards NNCI-2025489, NNCI-15421010), the Molecular Engineering & Sciences Institute, and the Clean Energy Institute; and the University of Washington Department of Chemistry. This research used resources of the Advanced Photon Source, a U.S. Department of Energy (DOE) Office of Science User Facility operated for the DOE Office of Science by Argonne National Laboratory under Contract No. DE-AC02-06CH11357.

The mail-in program at Beamline 17-BM contributed to the data. Finally, we gratefully acknowledge Dr. Samantha Young for assistance in collecting and analyzing XPS data and Dr. Adrienne Roehrich for assistance in collecting and analyzing solid-state NMR data.

References.

(1) Wang, S.; McGuirk, C. M.; d'Aquino, A.; Mason, J. A.; Mirkin, C. A. Metal–Organic Framework Nanoparticles. *Adv. Mater.* **2018**, *30* (37), 1800202. https://doi.org/10.1002/adma.201800202.

(2) Cai, X.; Xie, Z.; Li, D.; Kassymova, M.; Zang, S.-Q.; Jiang, H.-L. Nano-Sized Metal-Organic Frameworks: Synthesis and Applications. *Coordination Chemistry Reviews* **2020**, *417*, 213366. https://doi.org/10.1016/j.ccr.2020.213366.

(3) Ploetz, E.; Engelke, H.; Lächelt, U.; Wuttke, S. The Chemistry of Reticular Framework Nanoparticles: MOF, ZIF, and COF Materials. *Adv. Funct. Mater.* **2020**, *30* (41), 1909062. https://doi.org/10.1002/adfm.201909062.

(4) Cooper, A. I. Porous Molecular Solids and Liquids. *ACS Cent. Sci.* **2017**, *3* (6), 544–553. https://doi.org/10.1021/acscentsci.7b00146.

(5) Hosono, N.; Kitagawa, S. Modular Design of Porous Soft Materials via Self-Organization of Metal–Organic Cages. *Acc. Chem. Res.* **2018**, *51* (10), 2437–2446. https://doi.org/10.1021/acs.accounts.8b00361.

(6) Gosselin, A. J.; Rowland, C. A.; Bloch, E. D. Permanently Microporous Metal–Organic Polyhedra. *Chem. Rev.* **2020**, *120* (16), 8987–9014. https://doi.org/10.1021/acs.chemrev.9b00803.

(7) Strauss, M. J.; Evans, A. M.; Roesner, E. K.; Monsky, R. J.; Bardot, M. I.; Dichtel, W. R. Divergent Nanotube Synthesis through Reversible Macrocycle Assembly. *Acc. Mater. Res.* **2022**, *3* (9), 935–947. https://doi.org/10.1021/accountsmr.2c00062.

(8) Sánchez-González, E.; Tsang, M. Y.; Troyano, J.; Craig, G. A.; Furukawa, S. Assembling Metal–Organic Cages as Porous Materials. *Chem. Soc. Rev.* **2022**, *51* (12), 4876–4889. https://doi.org/10.1039/D1CS00759A.

(9) Zasada, L. B.; Guio, L.; Kamin, A. A.; Dhakal, D.; Monahan, M.; Seidler, G. T.; Luscombe, C. K.; Xiao, D. J. Conjugated Metal–Organic Macrocycles: Synthesis, Characterization, and Electrical Conductivity. *J. Am. Chem. Soc.* **2022**, *144* (10), 4515–4521. https://doi.org/10.1021/jacs.1c12596.

(10) Louie, S.; Zhong, Y.; Bao, S. T.; Schaack, C.; Montoya, A.; Jin, Z.; Orchanian, N. M.; Liu, Y.; Lei, W.; Harrison, K.; Hone, J.; Angerhofer, A.; Evans, A. M.; Nuckolls, C. P. Coaxially Conductive Organic Wires Through Self-Assembly. *J. Am. Chem. Soc.* **2023**, *145* (9), 4940–4945. https://doi.org/10.1021/jacs.2c12437.

(11) Pastore, V. J.; Cook, T. R. Coordination-Driven Self-Assembly in Polymer–Inorganic Hybrid Materials. *Chem. Mater.* **2020**, *32* (9), 3680–3700. https://doi.org/10.1021/acs.chemmater.0c00851.

(12) He, A.; Jiang, Z.; Wu, Y.; Hussain, H.; Rawle, J.; Briggs, M. E.; Little, M. A.; Livingston, A. G.; Cooper, A. I. A Smart and Responsive Crystalline Porous Organic Cage Membrane with Switchable Pore Apertures for Graded Molecular Sieving. *Nat. Mater.* **2022**, *21* (4), 463–470. https://doi.org/10.1038/s41563-021-01168-z.

(13) Jiang, Z.; Dong, R.; Evans, A. M.; Biere, N.; Ebrahim, M. A.; Li, S.; Anselmetti, D.; Dichtel, W. R.; Livingston, A. G. Aligned Macrocycle Pores in Ultrathin Films for Accurate

Molecular Sieving. *Nature* **2022**, *609* (7925), 58–64. https://doi.org/10.1038/s41586-022-05032-1.
(14) Gosselin, A. J.; Decker, G. E.; Antonio, A. M.; Lorzing, G. R.; Yap, G. P. A.; Bloch, E. D. A Charged Coordination Cage-Based Porous Salt. *J. Am. Chem. Soc.* **2020**, *142* (21), 9594–9598. https://doi.org/10.1021/jacs.0c02806.
(15) Jones, J. T. A.; Holden, D.; Mitra, T.; Hasell, T.; Adams, D. J.; Jelfs, K. E.; Trewin, A.; Willock, D. J.; Day, G. M.; Bacsa, J.; Steiner, A.; Cooper, A. I. On-Off Porosity Switching in a Molecular Organic Solid. *Angew. Chem. Int. Ed.* **2011**, *50* (3), 749–753. https://doi.org/10.1002/anie.201006030.
(16) Strauss, M. J.; Asheghali, D.; Evans, A. M.; Li, R. L.; Chavez, A. D.; Sun, C.; Becker, M. L.; Dichtel, W. R. Cooperative Self-Assembly of Pyridine-2,6-Diimine-Linked Macrocycles into Mechanically Robust Nanotubes. *Angew. Chem.* **2019**, *131* (41), 14850–14856. https://doi.org/10.1002/ange.201907668.
(17) Troyano, J.; Horike, S.; Furukawa, S. Reversible Discrete-to-Extended Metal–Organic Polyhedra Transformation by Sulfonic Acid Surface Functionalization. *J. Am. Chem. Soc.* **2022**, *144* (42), 19475–19484. https://doi.org/10.1021/jacs.2c07978.
(18) Guo, J.; Xu, Y.; Jin, S.; Chen, L.; Kaji, T.; Honsho, Y.; Addicoat, M. A.; Kim, J.; Saeki, A.; Ihee, H.; Seki, S.; Irle, S.; Hiramoto, M.; Gao, J.; Jiang, D. Conjugated Organic Framework with Three-Dimensionally Ordered Stable Structure and Delocalized π Clouds. *Nat Commun* **2013**, *4* (1), 2736. https://doi.org/10.1038/ncomms3736.
(19) Mahmood, J.; Lee, E. K.; Jung, M.; Shin, D.; Jeon, I.-Y.; Jung, S.-M.; Choi, H.-J.; Seo, J.-M.; Bae, S.-Y.; Sohn, S.-D.; Park, N.; Oh, J. H.; Shin, H.-J.; Baek, J.-B. Nitrogenated Holey Two-Dimensional Structures. *Nat Commun* **2015**, *6* (1), 6486. https://doi.org/10.1038/ncomms7486.
(20) Meng, Z.; Stolz, R. M.; Mirica, K. A. Two-Dimensional Chemiresistive Covalent Organic Framework with High Intrinsic Conductivity. *J. Am. Chem. Soc.* **2019**, *141* (30), 11929–11937. https://doi.org/10.1021/jacs.9b03441.
(21) Wang, M.; Ballabio, M.; Wang, M.; Lin, H.-H.; Biswal, B. P.; Han, X.; Paasch, S.; Brunner, E.; Liu, P.; Chen, M.; Bonn, M.; Heine, T.; Zhou, S.; Cánovas, E.; Dong, R.; Feng, X. Unveiling Electronic Properties in Metal–Phthalocyanine-Based Pyrazine-Linked Conjugated Two-Dimensional Covalent Organic Frameworks. *J. Am. Chem. Soc.* **2019**, *141* (42), 16810–16816. https://doi.org/10.1021/jacs.9b07644.
(22) Li, X.; Wang, H.; Chen, H.; Zheng, Q.; Zhang, Q.; Mao, H.; Liu, Y.; Cai, S.; Sun, B.; Dun, C.; Gordon, M. P.; Zheng, H.; Reimer, J. A.; Urban, J. J.; Ciston, J.; Tan, T.; Chan, E. M.; Zhang, J.; Liu, Y. Dynamic Covalent Synthesis of Crystalline Porous Graphitic Frameworks. *Chem* **2020**, *6* (4), 933–944. https://doi.org/10.1016/j.chempr.2020.01.011.
(23) Das, P.; Mandal, S. K. In-Depth Experimental and Computational Investigations for Remarkable Gas/Vapor Sorption, Selectivity, and Affinity by a Porous Nitrogen-Rich Covalent Organic Framework. *Chem. Mater.* **2019**, *31* (5), 1584–1596. https://doi.org/10.1021/acs.chemmater.8b04683.
(24) Ranjeesh, K. C.; Illathvalappil, R.; Veer, S. D.; Peter, J.; Wakchaure, V. C.; Goudappagouda; Raj, K. V.; Kurungot, S.; Babu, S. S. Imidazole-Linked Crystalline Two-Dimensional Polymer with Ultrahigh Proton-Conductivity. *J. Am. Chem. Soc.* **2019**, *141* (38), 14950–14954. https://doi.org/10.1021/jacs.9b06080.

(25) Zhou, R.; Huang, Y.; Li, Z.; Kang, S.; Wang, X.; Liu, S. Piperazine-Based Two-Dimensional Covalent Organic Framework for High Performance Anodic Lithium Storage. *Energy Storage Materials* **2021**, *40*, 124–138. https://doi.org/10.1016/j.ensm.2021.05.008.
(26) Yue, Y.; Li, H.; Chen, H.; Huang, N. Piperazine-Linked Covalent Organic Frameworks with High Electrical Conductivity. *J. Am. Chem. Soc.* **2022**, *144* (7), 2873–2878. https://doi.org/10.1021/jacs.1c13012.
(27) Smith, M. K.; Powers-Riggs, N. E.; Northrop, B. H. Rational Synthesis of Bis(Hexyloxy)-Tetra(Hydroxy)-Triphenylenes and Their Derivatives. *RSC Adv.* **2014**, *4* (72), 38281–38292. https://doi.org/10.1039/C4RA06503D.
(28) Sheberla, D.; Sun, L.; Blood-Forsythe, M. A.; Er, S.; Wade, C. R.; Brozek, C. K.; Aspuru-Guzik, A.; Dincă, M. High Electrical Conductivity in Ni3(2,3,6,7,10,11-Hexaiminotriphenylene)2, a Semiconducting Metal–Organic Graphene Analogue. *J. Am. Chem. Soc.* **2014**, *136* (25), 8859–8862. https://doi.org/10.1021/ja502765n.
(29) Chen, T.; Dou, J.-H.; Yang, L.; Sun, C.; Libretto, N. J.; Skorupskii, G.; Miller, J. T.; Dincă, M. Continuous Electrical Conductivity Variation in M $_3$ (Hexaiminotriphenylene) $_2$ (M = Co, Ni, Cu) MOF Alloys. *J. Am. Chem. Soc.* **2020**, *142* (28), 12367–12373. https://doi.org/10.1021/jacs.0c04458.
(30) Day, R. W.; Bediako, D. K.; Rezaee, M.; Parent, L. R.; Skorupskii, G.; Arguilla, M. Q.; Hendon, C. H.; Stassen, I.; Gianneschi, N. C.; Kim, P.; Dincă, M. Single Crystals of Electrically Conductive Two-Dimensional Metal–Organic Frameworks: Structural and Electrical Transport Properties. *ACS Cent. Sci.* **2019**, *5* (12), 1959–1964. https://doi.org/10.1021/acscentsci.9b01006.
(31) Dou, J.-H.; Arguilla, M. Q.; Luo, Y.; Li, J.; Zhang, W.; Sun, L.; Mancuso, J. L.; Yang, L.; Chen, T.; Parent, L. R.; Skorupskii, G.; Libretto, N. J.; Sun, C.; Yang, M. C.; Dip, P. V.; Brignole, E. J.; Miller, J. T.; Kong, J.; Hendon, C. H.; Sun, J.; Dincă, M. Atomically Precise Single-Crystal Structures of Electrically Conducting 2D Metal–Organic Frameworks. *Nature Materials* **2021**, *20* (2), 222–228. https://doi.org/10.1038/s41563-020-00847-7.
(32) Xie, L. S.; Skorupskii, G.; Dincă, M. Electrically Conductive Metal–Organic Frameworks. *Chem. Rev.* **2020**, *120* (16), 8536–8580. https://doi.org/10.1021/acs.chemrev.9b00766.
(33) Sheberla, D.; Bachman, J. C.; Elias, J. S.; Sun, C.-J.; Shao-Horn, Y.; Dincă, M. Conductive MOF Electrodes for Stable Supercapacitors with High Areal Capacitance. *Nature Mater* **2017**, *16* (2), 220–224. https://doi.org/10.1038/nmat4766.
(34) Miner, E. M.; Fukushima, T.; Sheberla, D.; Sun, L.; Surendranath, Y.; Dincă, M. Electrochemical Oxygen Reduction Catalysed by Ni3(Hexaiminotriphenylene)2. *Nat Commun* **2016**, *7* (1), 10942. https://doi.org/10.1038/ncomms10942.
(35) Mariano, R. G.; Wahab, O. J.; Rabinowitz, J. A.; Oppenheim, J.; Chen, T.; Unwin, P. R.; Dincă, M. Thousand-Fold Increase in O $_2$ Electroreduction Rates with Conductive MOFs. *ACS Cent. Sci.* **2022**, *8* (7), 975–982. https://doi.org/10.1021/acscentsci.2c00509.
(36) Smith, M. K.; Mirica, K. A. Self-Organized Frameworks on Textiles (SOFT): Conductive Fabrics for Simultaneous Sensing, Capture, and Filtration of Gases. *J. Am. Chem. Soc.* **2017**, *139* (46), 16759–16767. https://doi.org/10.1021/jacs.7b08840.
(37) Ko, M.; Mendecki, L.; Eagleton, A. M.; Durbin, C. G.; Stolz, R. M.; Meng, Z.; Mirica, K. A. Employing Conductive Metal–Organic Frameworks for Voltammetric Detection of Neurochemicals. *J. Am. Chem. Soc.* **2020**, *142* (27), 11717–11733. https://doi.org/10.1021/jacs.9b13402.

(38) Matienzo, J.; Yin, L. I.; Grim, S. O.; Swartz, W. E. X-Ray Photoelectron Spectroscopy of Nickel Compounds. *Inorg. Chem.* **1973**, *12* (12), 2762–2769. https://doi.org/10.1021/ic50130a005.
(39) Stolz, R. M.; Mahdavi-Shakib, A.; Frederick, B. G.; Mirica, K. A. Host–Guest Interactions and Redox Activity in Layered Conductive Metal–Organic Frameworks. *Chem. Mater.* **2020**, *32* (18), 7639–7652. https://doi.org/10.1021/acs.chemmater.0c01007.
(40) Artyushkova, K. Misconceptions in Interpretation of Nitrogen Chemistry from X-Ray Photoelectron Spectra. *Journal of Vacuum Science & Technology A: Vacuum, Surfaces, and Films* **2020**, *38* (3), 031002. https://doi.org/10.1116/1.5135923.
(41) Chavez, A. D.; Smith, B. J.; Smith, M. K.; Beaucage, P. A.; Northrop, B. H.; Dichtel, W. R. Discrete, Hexagonal Boronate Ester-Linked Macrocycles Related to Two-Dimensional Covalent Organic Frameworks. *Chem. Mater.* **2016**, *28* (14), 4884–4888. https://doi.org/10.1021/acs.chemmater.6b01831.
(42) Lukose, B.; Kuc, A.; Heine, T. The Structure of Layered Covalent-Organic Frameworks. *Chemistry A European J* **2011**, *17* (8), 2388–2392. https://doi.org/10.1002/chem.201001290.
(43) Kang, C.; Zhang, Z.; Wee, V.; Usadi, A. K.; Calabro, D. C.; Baugh, L. S.; Wang, S.; Wang, Y.; Zhao, D. Interlayer Shifting in Two-Dimensional Covalent Organic Frameworks. *J. Am. Chem. Soc.* **2020**, *142* (30), 12995–13002. https://doi.org/10.1021/jacs.0c03691.
(44) Wu, X.; Han, X.; Liu, Y.; Liu, Y.; Cui, Y. Control Interlayer Stacking and Chemical Stability of Two-Dimensional Covalent Organic Frameworks via Steric Tuning. *J. Am. Chem. Soc.* **2018**, *140* (47), 16124–16133. https://doi.org/10.1021/jacs.8b08452.
(45) Bian, G.; Yin, J.; Zhu, J. Recent Advances on Conductive 2D Covalent Organic Frameworks. *Small* **2021**, *17* (22), 2006043. https://doi.org/10.1002/smll.202006043.
(46) Yang, Y.; Börjesson, K. Electroactive Covalent Organic Frameworks: A New Choice for Organic Electronics. *Trends in Chemistry* **2022**, *4* (1), 60–75. https://doi.org/10.1016/j.trechm.2021.10.007.
(47) Smith, B. J.; Parent, L. R.; Overholts, A. C.; Beaucage, P. A.; Bisbey, R. P.; Chavez, A. D.; Hwang, N.; Park, C.; Evans, A. M.; Gianneschi, N. C.; Dichtel, W. R. Colloidal Covalent Organic Frameworks. *ACS Cent. Sci.* **2017**, *3* (1), 58–65. https://doi.org/10.1021/acscentsci.6b00331.
(48) Zhao, Y.; Guo, L.; Gándara, F.; Ma, Y.; Liu, Z.; Zhu, C.; Lyu, H.; Trickett, C. A.; Kapustin, E. A.; Terasaki, O.; Yaghi, O. M. A Synthetic Route for Crystals of Woven Structures, Uniform Nanocrystals, and Thin Films of Imine Covalent Organic Frameworks. *J. Am. Chem. Soc.* **2017**, *139* (37), 13166–13172. https://doi.org/10.1021/jacs.7b07457.
(49) Khalil, S.; Meyer, M. D.; Alazmi, A.; Samani, M. H. K.; Huang, P.-C.; Barnes, M.; Marciel, A. B.; Verduzco, R. Enabling Solution Processable COFs through Suppression of Precipitation during Solvothermal Synthesis. *ACS Nano* **2022**, *16* (12), 20964–20974. https://doi.org/10.1021/acsnano.2c08580.